

Conducted Emission Prediction within the Network Based on Switching Impedances and EMI Sources

Achour Ales^{1, *}, Mohamed A. Cheurfi Belhadj¹,
Abdelhalim Zaoui¹, and Jean-Luc Schanen²

Abstract—Since electromagnetic compatibility studies intend to predict the compliance with electromagnetic standards, an accurate computation of both common and differential mode conducted noises is necessary. Modern networks such as in automobiles that are known for supplying many electrical actuators — include many power converters and long cables (conductors) to efficiently manage power transfer. However, the presence of both converters and cables creates new electromagnetic compatibility issues. For example, the interaction between cables and converters becomes a noise source. For this reason electromagnetic compatibility study becomes more complex. Therefore, the purpose of this paper is an attempt to propose an analytical model that computes noise sources by generating conducted signals within the network at any site, meaning all along the cable according to the CISPR16 standard. Our approach primarily consists of modeling conducted noise sources generated by converters connected to the DC-network which are extracted and identified in both frequency and time domains. The electromagnetic compatibility modelling of converter's behaviour is performed by defining a mathematical switching function. The model is assessed with time domain simulations and identified by experimental measurements. Secondly, the extracted converter's model, based on equivalent noise sources, is used to predict the conducted noise inside a defined network at any location of the cable. The process of the network's modelling is realised through using the Multi-Transmission Line Method of lossless lines. This network's model is crucial for EMC analysis in order to evaluate the interaction degree between noise sources and cable parameters.

1. INTRODUCTION

Nowadays, electric power and applied smart systems — such as in avionic and vehicle structures, power distribution, and aerospace — tend to be in more and more mobile applications, electric actuators, and digital processing core, supplied by power converters. This electrical trend offers many advantages. On one hand, it is good for the dynamic of the systems. On the other hand, it offers better comfort for persons. However, it contributes to creating undesirable ElectroMagnetic (EM) phenomena which decrease system reliability [1, 2]. However, power electronics converters aboard embedded systems are potential source of ElectroMagnetic Interferences (EMI) across a wide frequency band, which can interact with other systems meaning propagation paths, mainly *cables* and *electrical tracks* [3–5]. Hence, during designing and for an optimal manufacturing cost and size point of view, it is important to account for the ElectroMagnetic Compatibility (EMC) constraints. In addition, within modern multisource grids — as in photovoltaic systems — common mode (CM) current, mainly flowing inside shielding structures, may cause serious safety risks, dysfunctions, and saturation effects inside magnetic circuit of EMI filters [6–10].

Received 29 January 2019, Accepted 29 July 2019, Scheduled 6 September 2019

* Corresponding author: Achour Ales (achour.ales@gmail.com).

¹ Polytechnic Military School, Bordj-El-Bahri, Algiers 16111, Algeria. ² G2ELab, University of Grenoble, Bat Ense3 BP46 F-38402 SMH Cedex, Grenoble, France.

Generally, to attenuate EM emissions, engineers act on two entities: EMI sources such as power electronics converters or the coupling path -mainly cables- which fix the whole impedance of the system in both CM and Differential Mode (DM) references [11]. For that reason, the accurate prediction of EMI emissions is crucial, not only for EMI filters design and optimisation but also conforming to EMC standards, as the German VDE 0126-1-1 standard, DO-160 aerospace standard, and DO-160 category “B” which requires a specific aeronautic *Line Impedance Stabilization Network* (LISN) [11].

Several works focus on modeling the EMI prediction on systems integrated electronics power converters, because of their high level of di/dt and dv/dt , which is the origin of the EM emissivity [12]. First, physics-based model identified by experimental and software tests requires an inordinate amount of simulation time [13]. Secondly, the Black-Box system approach based on experimental identification cannot reveal actual parameters’ impact [14]. The predictive and modular terminal behavioural models which consist of estimating the global internal noise’s source are not suitable for cascading topologies [15–17]. The quadripolar matrices approach cannot estimate the DM emission [18,19]. Finally, the unterminated EMI models need a lot of simulation time [20].

To sum up, the rise electrification of the embedded systems caused by the growth of the cables’ densities increases the complexity and cumbersomeness. Therefore, converter’s noise source prediction is crucial to show how the EM emission respects EMC standards. However, this is not necessarily sufficient to reduce the risk, especially in case that the converters are connected via long cables, because cables are the excellent transmitters of EMI emissions and also increase conducted interferences due to resonances and propagation phenomena related to the per-unit conductors’ parameters “ $l.dx$, $c.dx$ and $r.dx$ ” (see Fig. 1). The most used techniques in this field to perform an accurate EMC analysis are the Transmission Line Method (TLM) [21]. There are many applied subjects based on that theory, for instance to model grounding conductors [22], to analyse the radiated and conducted susceptibility of multi-conductor shielded cables [23], also in order to optimise EMI filters, so as considering length cable influence on the filter insertion loss [24]. On the other hand, within the network, because of the propagation phenomena inside conductors, the conducted noise magnitude differs from point to another, which can also be attributed to the cables’ parameters [25].

The main purpose of this work is to formulate an EMC comprehensive model of a defined network, including long cables accordingly with the EMC standard CISPR16. The model depends on the cables’ physical, geometrical, and technological parameters, which allows us to predict the conducted noise EMI and the coupling path (impedances) at any position “ P_i ” inside the network, as depicted in Fig. 1. Therefore, the study will be performed in both cases: the DM and the CM references.

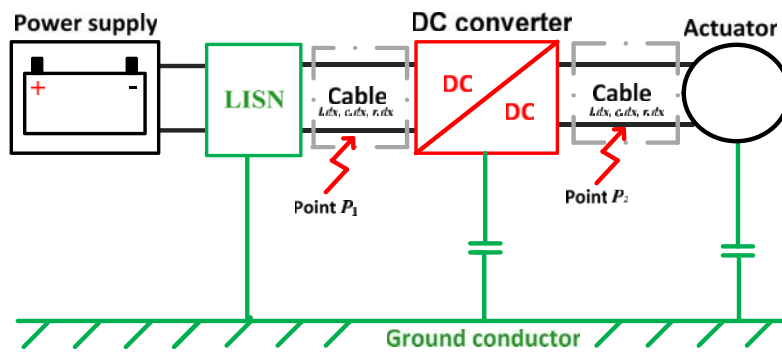


Figure 1. Synoptic scheme of a DC-grid.

As an illustration, within an embedded electrical grid — as shown in Fig. 1 — the conducted noise’s magnitude differs from *point* to other (“ P_i ” $i = \{1,2\}$), because of the cable’s impedances which depend on measurement on that point “ P_i ”. Therefore, new resonances may appear, and subsequently the conducted disturbances become non-compliant with EMC standards level, which forces engineers to redesign EMC filters.

The reduced computing time is the main benefit of the analytical-based method which is suitably used in efficient algorithms devoted to designing reduced volume EMI filters. Moreover, they allow a

topology modification impact versus a voltage fluctuation inside the nodal topology. That model is helpful for understanding EMI dependency on the network’s parameters (converters and cables). It is also intended to reduce security margins applied to filters’ design, which generally increase the cost and size.

This paper will be organised as follows:

Firstly, we expose the mathematical model of the buck converter (Fig. 3). Based on the analysis, the extracted model provides the coupling path in both the DM and CM noise and also offers an EMI noise sources model. Secondly, the converter model is used to model the whole network, as defined in Fig. 1. Subsequently, the model helps us to understand the sources’ noise (of the converter) behaviour when we are in a position farther away from the noise source (e.g., at the point “ P_i ” $i = \{1, 2\}$ in Fig. 1). It is also important to highlight that this network model is extracted using the TLM theory, assessed by a temporal simulation and identified by experimental measurements.

2. GENERAL PURPOSE

2.1. Issues Description

Nowadays, since cables are crucial elements within embedded systems, an EMC analysis — especially about the cables’ behaviour in EMC point of view — is highly needed to improve systems reliability and reduce the cumbersomeness. The TLM theory is one of the efficient applied methods, which consists in partitioning cable’s conductors into small elements — much smaller than one tenth of wavelength — where a propagation phenomenon is neglected [26]. Each element will be modelled by a transmission line (TL) cell characterized by losses as illustrated in [17].

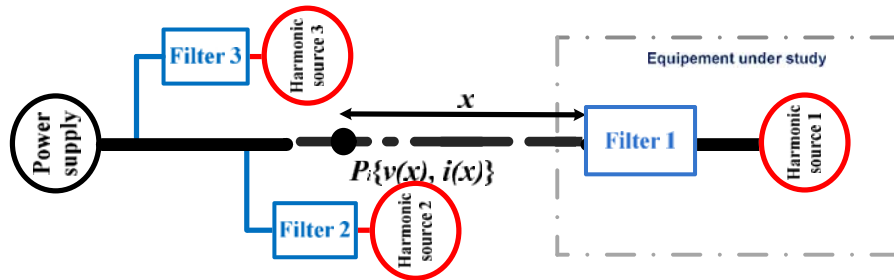


Figure 2. A synoptic scheme of a DC network.

Figure 2 is the global representation of the network drawn in Fig. 1, considering many power electronics converters, modelled by their equivalent *harmonic sources* including their own input EMI *filter*. Hence, the noise generated by the “*harmonic sources 1*” is attenuated by the “*Filter 1*”. However, once this filtered noise $\{v, i\}$ crosses the distance “ x ” until the point “ P_i ” $\{v(x), i(x)\}$, new resonances may appear due to propagation phenomena and per-unit parameters “ $l.dx, c.dx, r.dx$ ”, according to the law expressed in Eq. (1) [21]. Once more, according to Eq. (1), the filtered noise becomes not compliant with EMC standards. For this purpose, in order to remain compliant with EMC regulations, the efforts in this work are steered towards the formulation of an EMC comprehensive model of a network, depending on its intrinsic physical and geometrical parameters, so as to be able to predict the conducted noise EMI not only at the two extremities of the network but also at any site “ P_i ” inside the network, as depicted in Fig. 2. This model will be realized in both DM and CM cases. The main reasons are to highlight the EMI noise dependency on the network’s parameters (converters and cables) to help engineers at the design filters stage and not to help users at the default diagnostic process.

$$v(x) = \cos(\beta \cdot x) \cdot V_{conv} - j \cdot Z_c \sin(\beta \cdot x) \cdot I_{conv} \tag{1}$$

where:

- x : is the distance crossed by the harmonic current (or voltage) inside the network regarding the converter;

- Z_c : is the characteristic impedance of the cable [21];
- β : is the propagation constant [21];
- V_{conv} and I_{conv} : are respectively harmonic voltage and current generated by the converter when operating;
- j : is the complex number.

2.2. The System under Study

The network under study (Fig. 1) contains battery power supply, LISN, a buck converter (Fig. 3), “ RL ” load and cables. The buck converter under study is a DC-DC converter which allows the DC voltage to decrease, thanks to the switching operation of the “ S ” device (as depicted in Fig. 3). Accordingly, the diode and device “ S ” work in a complementary way, which permit the input voltage chopping and consequently decrease it at the output side according to a defined duty cycle α . The buck converter is a *Linear and Time Invariant* (LTI) system [17, 27], which means that the electrical equations are based on circuit theory. As depicted in Fig. 3, essential coupling paths are considered, including imperfections of different passive components (load, input capacitor C_f), imperfections of switching devices (C_{ds} and C_d), and essential parasitical elements of the converter’s PCB, such as parasitical capacities to the ground and line parasitical inductances.

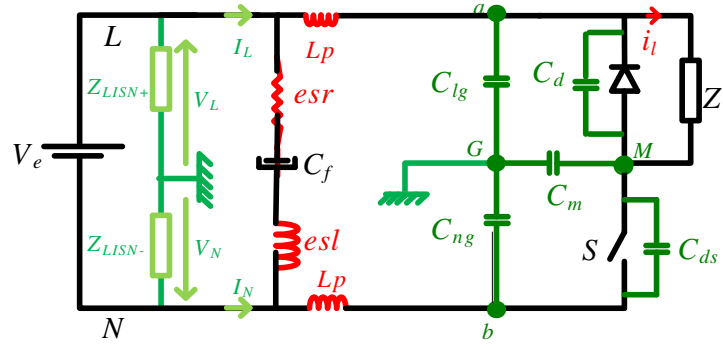


Figure 3. Buck circuit under study

2.3. Switching Function

The analytical model developed in this work is built thanks to the periodical switching function $g_{sw}(t)$ illustrated in Fig. 4, which defines the switching behaviour of the buck converter. This function illustrates when the converter is in the state “ ON ” (then all parameters will be indexed by “1”), and when it is “ OFF ” (then all parameters will be indexed by “0”). For example, all impedances, when

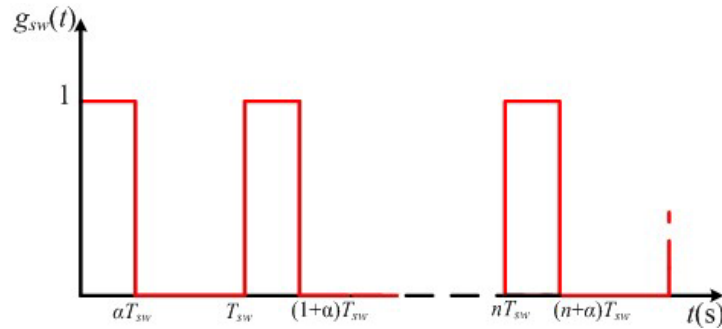


Figure 4. The switching function.

the converter is “ON”, will be as “ Z_1 ”; “ Z_0 ” for the other state. The frequency of $g_{sw}(t)$ corresponds to the switching frequency of the converter “ $F_{sw} = 1/T_{sw}$ ”.

3. THE DIFFERENTIAL MODE MODEL OF THE CONVERTER

Usually, the DM current (or voltage) is the quantity of the signal flowing inside circuits, from “ L -line” to “ N -line”, without including the ground conductor “ G ”, as depicted in Fig. 5(a) and expressed in Eq. (2).

$$\begin{aligned} \begin{pmatrix} I_{dm} \\ I_{cm} \end{pmatrix} &= [M_i] \cdot \begin{pmatrix} I_L \\ I_N \end{pmatrix}, & [M_i] &= \begin{pmatrix} \frac{1}{2} & -\frac{1}{2} \\ 1 & 1 \end{pmatrix} \\ \begin{pmatrix} V_{dm} \\ V_{cm} \end{pmatrix} &= [M_v] \cdot \begin{pmatrix} V_L \\ V_N \end{pmatrix}, & [M_v] &= \begin{pmatrix} 1 & -1 \\ \frac{1}{2} & \frac{1}{2} \end{pmatrix} \end{aligned} \quad (2)$$

The aim of this section is to formulate a predictive analytical model, based on a quadripolar system to be able to compute the conducted noise amount that may be filtered by the DM filter in order to facilitate the EMI prediction within the electrical grid.

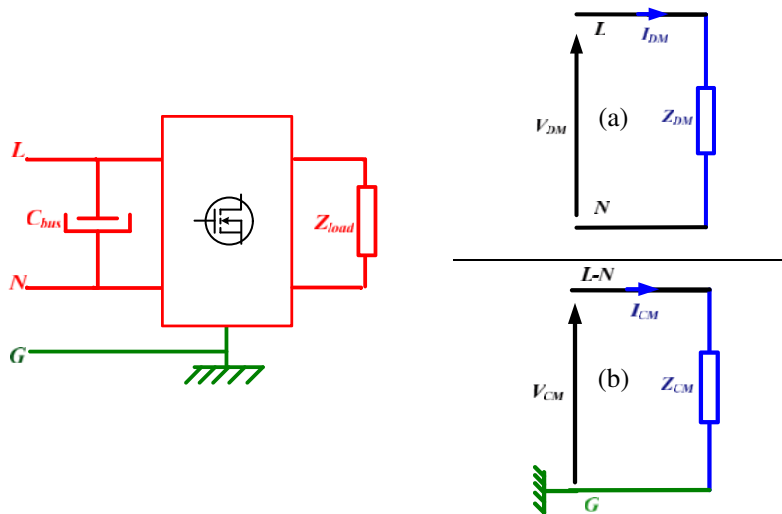


Figure 5. The converter model: (a) The differential mode model. (b) The common mode model.

3.1. Circuit Model of the Converter

Regarding the DM reference, the converter of Fig. 3 can be schematised by an equivalent circuit as depicted in Fig. 6 [28]. Accordingly, the whole converter may be represented by two types of impedances between the two lines’ wire L - N : the parallel impedance Z_p (parallel with the controlled switch $g_{sw}(t)$) and the serial impedance Z_s (serial with the controlled switch $g_{sw}(t)$), as illustrated in Fig. 6. Note that this circuit can be finally represented by a *Norton* (or *Thevenin*) equivalent circuit, as depicted in Fig. 7(a) and Fig. 7(b) [28]. The input current of the model at the frequency domain is expressed in Eq. (3) [28], where Y_{DM} is the DM admittance of the circuit as expressed in Eq. (4) [29].

$$I_e(f) = Y_{DM} \cdot V_e(f) + I_h(f) \quad (3)$$

$$Y_{MD,MC} = \frac{I_{MD,MC}}{V_{MD,MC}} \quad (4)$$

where: $Z_{DM} = \frac{1}{Y_{DM}}$ and $V_h = \frac{1}{Y_{DM}} \cdot I_h$.

- $V_e(f - (xn + k)x \cdot F_{sw})$ are the harmonic components of the input voltage, due to the power devices' switching.

$$I_h(f) = \alpha^2 \cdot A_{n,k}(f, \alpha) \cdot V_e(f - (n + k)F_{sw}) \tag{10}$$

$$Y_{DM} = Y_p(f) + \alpha^2 \cdot \sum \sin^2(\pi n\alpha) \cdot Y_s(f - nF_{sw}) \tag{11}$$

$$A_{n,k}(f, \alpha) = \left(\sum_n \sum_{\substack{k \\ n+k \neq 0}} \frac{\alpha^2 \cdot \text{sinc}(\pi n\alpha) \cdot \text{sinc}(\pi k\alpha)}{Z_s(f - nF_{sw})} \cdot e^{-j\pi\alpha(n+k)} \right) \tag{12}$$

According to Eq. (10), the harmonic current I_h , under the previous assumptions, depends on the harmonic components of $V_e(f)$ biased by coefficients “ $A_{n,k}$ ” expressed in Eq. (13), which are dependent on the converter’s switching operation, such as the duty cycle α and serial impedance Z_s . This proves to a certain degree —although based on advanced assumptions— that the equivalent noise source representing the converter behaviour is a-priori the signal on the switching devices sides chopped at the switching frequency F_{sw} . This joins some endorsed previous models such as in [19, 9].

4. DIFFERENTIAL MODE PARAMETERS’ IDENTIFICATION OF THE CONVERTER MODEL

The DM converter model represented by Z_s and Z_p impedances (Equations (3), (10), and (11)) has to be identified by computing these parameters. Actually, these impedances depend on passive components and parasitical elements of the converter (see Fig. 3), such as the input capacitor C_f including its parasitical elements, impedance load Z_l , line parasitical inductances L_p , capacitances to the ground C_{lg} , C_{ng} , and C_m .

4.1. Parameter Identification Process

The DM model of the converter is set by two impedances which have to be identified: Z_s and Z_p . They are expressed with two equivalent impedances of the converter when the switch is “OFF”: $g_{sw}(t) = 0$, so the whole converter impedance $Z_{converter} = Z_{LN0}$, or when it is “ON”: $g_{sw}(t) = 1$ so $Z_{converter} = Z_{LN1}$, as established in [19]. Therefore, according to $g_{sw}(t)$ states in Fig. 6 (see Fig. 4), the relationship between the impedances is as bellow:

$$Z_p = Z_{LN0}, \quad \text{the switch is “OFF” } (g_{sw}(t) = 0) \tag{13}$$

$$Z_s = \frac{1}{\frac{1}{Z_{LN1}} - \frac{1}{Z_{LN0}}}, \quad \text{the switch is “ON” } (g_{sw}(t) = 1) \tag{14}$$

Note that both Z_{LN0} and Z_{LN1} impedances depend on passive components and parasitical elements of the converter, which will be identified in in Eqs. (15) and (16) [19], where Z_{Lp} , Z_{Clg} , Z_{Cng} , Z_{Cm} are respectively the impedances of the parasitical elements L_p , C_{lg} , C_{ng} , and C_m depicted in Fig. 3.

$$Z_{LN0} = 2 \cdot Z_{Lp} + \frac{1}{Y_{C_{lg}} + Y_{C_m}} + Z_{C_{ng}} \tag{15}$$

$$Y_{LN1} = Y_L + \frac{Y_{C_{ng}} + Y_{C_m}}{1 + Z_{C_{lg}}(Y_{C_{ng}} + Y_{C_m})} \tag{16}$$

Figure 8 shows the impedance profile of Z_{LN0} corresponding to different switches (*Mosfet*) technologies. The point that we would like to clarify is that the *Mosfet*’s technology has an effect on the EMI’s coupling path. This means that resonances due to the converter’s impedance are nearly dependent on the switchers’ technology.

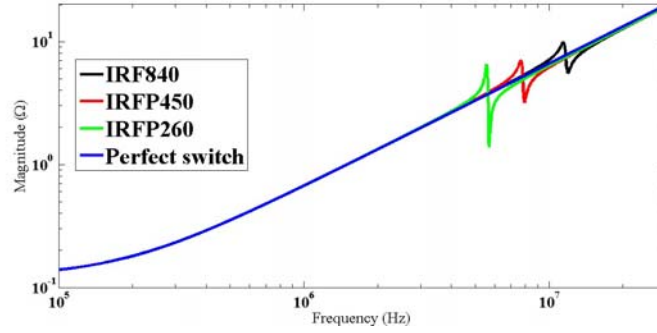


Figure 8. The frequency profile of Z_{LN0} impedance for different *Mosfet's* technology of the buck converter under study.

4.2. Input Capacitor C_f

The input capacitor's impedance Z_{Cf} of the buck converter is modelled by three serial elements: the capacitance C_f , serial inductor element “*esl*”, and serial resistive element “*esr*” represented in the converter topology of Fig. 3, and values are listed in Table 1. The identification of the three parameters is achieved by an impedance analyser “*WK 6500B*”. The resulting model is traced in Fig. 9.

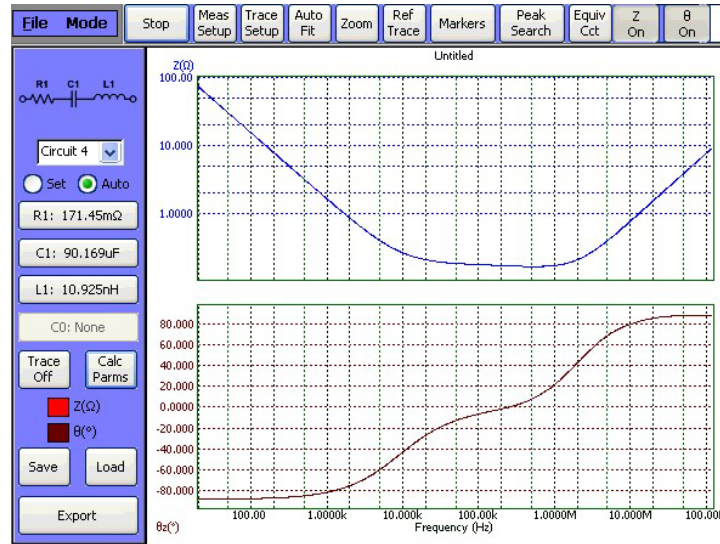


Figure 9. The input capacitor's impedance with the phasal.

4.3. Line Parasitical Inductances

Regardless of the printed circuit “*PCB*”, there are always parasitical inductances “ L_p ” from the copper track. The line parasitical inductances taken into account in the *PCB* of the buck converter (Fig. 3) are between the switching cell and input capacitor because of their hard contribution to EMC constraint [30]. They are estimated by “*FEMM*” software and measured by the impedance analyser “*WK 6500B*”. Results are shown in Table 1.

4.4. Parallel and Serial Impedances

The parallel and serial impedances included in the *DM* model of the converter (Fig. 6) are deduced from passive components previously identified and are drawn in Fig. 10. Note that impedances Z_p and

Table 1.

Converter elements	Measure	Parasitical elements	Simulation	Measure
C_f	98 μF	esl	-	135 nH
L	1.61 mH	esr		127.3 m Ω
R_l	12 Ω	l_p	92 nH	100 nH
		C_m	50 pF	35 pF
		C_{lg}	1 pF	14 pF
		C_{ng}	10 pF	14 pF
		load parasitical capacitance	-	456 pF

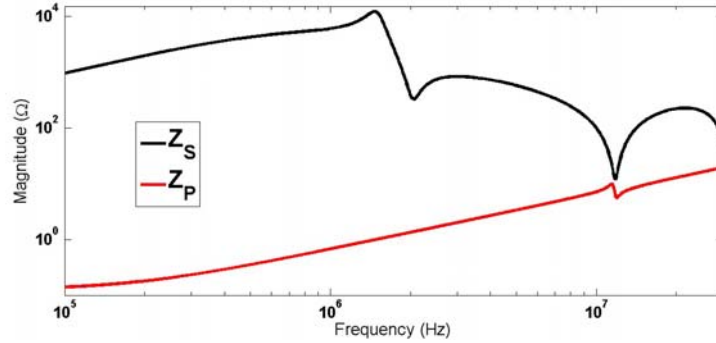


Figure 10. Parallel (Z_p) and serial (Z_s) impedances spectrum.

Z_s are almost equal around 12 MHz. This frequency may produce a resonance for the current profile. Hence, it is the subject of the next section.

5. THE COMMON MODE MODEL OF THE CONVERTER

5.1. The Circuit Model

The CM current (or voltage) is the quantity of the signal including the reference conductor (G) as coupling path, as depicted in Fig. 5(b) and expressed in Eq. (2). Accordingly, this section will be dedicated to formulate the amount of conducted noise that may be filtered by the CM filter.

5.2. The Mathematical Model of the Converter

The model to extract is also achieved by the switching function $g_{sw}(t)$ (see Fig. 4). The aim is to compute the CM current, which exclusively circulates inside the reference conductor “ G ”. As achieved in the DM case, the whole converter for the CM may be represented by four impedances, parallels’ impedances to the ground: Z_{pgp} and Z_{ngp} (parallel with the controlled switch $g_{sw}(t)$) and serials’ impedances Z_{pgs} and Z_{ngs} (serial with the controlled switch $g_{sw}(t)$), as illustrated in Fig. 11.

The CM current I_{CM} of the reference conductor “ G ” is the sum of both lines’ currents I_{cmp} and I_{cmn} (Fig. 11) as expressed in Eq. (17). V_L and V_N are the lines’ voltages to the ground as depicted in Fig. 11.

$$I_{CM} = I_{cmp} + I_{cmn} \tag{17}$$

$$I_{cmp} = (Y_{pgp} + Y_{pgs}) \cdot V_L - Y_{pgs} \cdot (G(f) \otimes V_L) \tag{18}$$

$$I_{cmn} = Y_{ngp} \cdot V_N + Y_{ngs} \cdot (G(f) \otimes V_N) \tag{19}$$

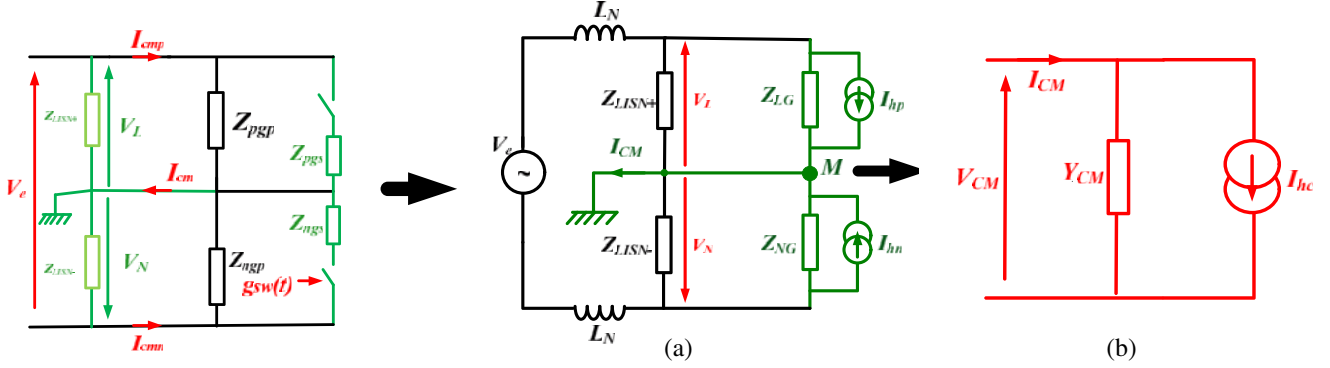


Figure 11. CM impedances model of the converter including switchers: (a) The converter quadripole model regarding the CM base. (b) The CM model of the buck converter with the equivalent current source.

The development of Equation (17) yields the CM current expressed in Eq. (20) with the CM admittance Y_{CM} and converter's parameters.

$$I_{CM} = Y_{CM} \cdot V_{CM} + Y_{DMC} \cdot \frac{V_{DM}}{2} - I_{DMh} - I_{CMh} \quad (20)$$

$$Y_{CM} = Y_{pgp} + Y_{ngp} + Y_{pgs} - \alpha \cdot (Y_{ngs} - Y_{pgs}) \quad (21)$$

$$Y_{DMC} = Y_{pgp} - Y_{ngp} + Y_{pgs} - \alpha \cdot (Y_{ngs} + Y_{pgs}) \quad (22)$$

$$I_{DMh} = \alpha \cdot \frac{(Y_{ngs} + Y_{pgs})}{2} \cdot \sum_{n \neq 0} \sin c(\pi n \alpha) \cdot e^{-j\pi \alpha n} \cdot V_{DM} (f - n \cdot F_{sw}) \quad (23)$$

$$I_{CMh} = \alpha \cdot (Y_{ngs} - Y_{pgs}) \cdot \sum_{n \neq 0} \sin c(\pi n \alpha) \cdot e^{-j\pi \alpha n} \cdot V_{CM} (f - n \cdot F_{sw}) \quad (24)$$

where:

- $G(f) \otimes V_n(f)$ is the convolution product.
- I_{DMh} and I_{CMh} are the noise currents' components generated by the buck converter.

Since the converter model is developed under the separation mode assumption [19], the DM voltage is supposed to be zero ($V_{DM} = 0$). As a result, the current in Eq. (23) is zero, and the CM current is reduced as expressed in Eq. (25).

$$I_{CM} = Y_{CM} \cdot V_{CM} - I_{CMh} \quad (25)$$

6. COMMON MODE PARAMETERS' IDENTIFICATION OF THE CONVERTER MODEL

The CM converter model has to be identified by computing Z_{pgs} , Z_{ngs} , Z_{pgp} , and Z_{ngp} . Actually, these impedances depend on when the switch converter is "OFF" or "ON", as realised in the DM case: Z_{LN0} , Z_{LN1} , Z_{LG0} , Z_{LG1} , Z_{NG0} , and Z_{NG1} , and also depend on passive components and parasitical elements of the converter (see Fig. 11), such as the input capacitor C_f including its parasitical elements, load impedance Z_l , line parasitical inductances L_p , capacitances to the ground C_{lg} , C_{ng} , and C_m . According to Fig. 11, the expressions of converter impedances are given below:

$$Y_{pgp} = Y_{LG1} - Y_p - Y_s \quad (26)$$

$$Y_{pgs} = Y_{LG0} - Y_{LG1} + Y_s \quad (27)$$

$$Y_{ngp} = Y_{NG0} - Y_p \quad (28)$$

$$Y_{ngs} = Y_{NG1} - Y_{NG0} - Y_s \quad (29)$$

6.1. Parasitical Capacitances to the Ground

The parasitical capacitances to the ground C_{lg} , C_{ng} , and C_m are deduced from three measurement profiles by the impedance analyser “WK 6500B”, according to the converter topology [31]:

- Z_{LG} : impedance between *Plus-Ground* wires,
- Z_{NG} : impedance between *Minus-Ground* wires,
- Z_{LN} : impedance between *Plus-Minus* wires.

The parameters are also computed using FEMM software and shown in Table 1. Note that there is no big difference between experimental and software results.

6.2. Parallel and Serial Impedances

Once the converter parameters are identified, the parallel and serial impedances (Equations (26)–(29)), as depicted in Fig. 11, are drawn in Fig. 12. It is important to point out that for the CM case, the resonance appears around 29 MHz.

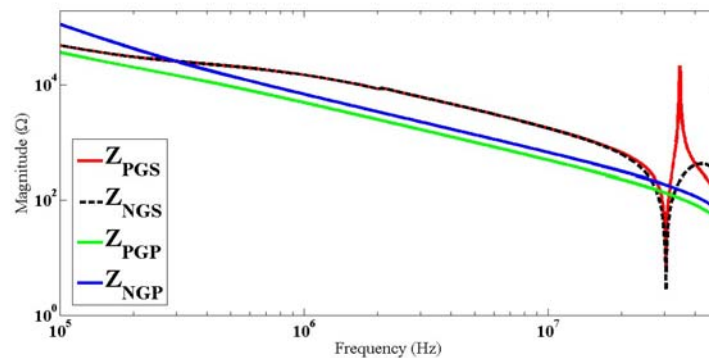


Figure 12. Parallel and serial impedances spectrum.

6.3. Common Mode Impedance

According to the previous identification of parameters, the CM impedance of Equation (21) is traced in Fig. 13 and compared to *LtSpice* simulation. The spectrum profile is mainly capacitive owing to parasitical capacitances to the ground [31]. Note that the resonance frequency for this impedance appears around 29 MHz also identical with that of the parallel and serial impedances of Fig. 12.

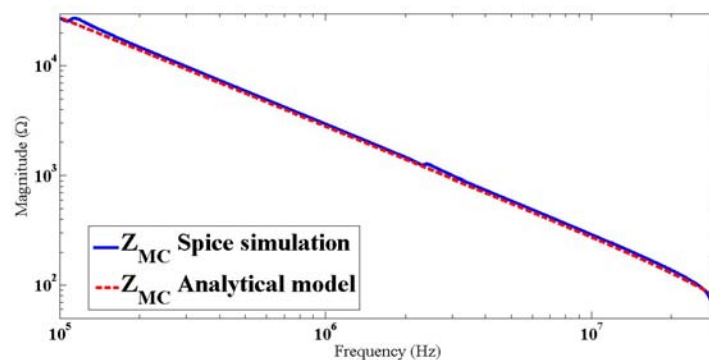


Figure 13. The CM impedance of the converter under test.

7. TIME DOMAIN SIMULATION OF THE CONVERTER MODEL

In order to test the developed model of the buck converter (Fig. 3) in both DM and CM references developed respectively in Eqs. (8) and (25), we have performed a time domain simulation using *LTspice* software. The buck converter is introduced into the software with consideration of all essential coupling elements [30]: the layout inductance l_p , parasitical capacitances to the ground C_{pg} , C_{ng} and C_m , and the switching devices capacitances (C_d for the *diode* and C_{ds} for the *Mosfet*). The simulation is achieved under the following operation points: Input DC voltage: $E = 100$ V, Switching frequency: $F_{sw} = 10$ kHz, Duty cycle: $\alpha = 0.3$.

In order to perform the current capture, we have used a 5-LISN to separate both CM and DM currents. The DM current is estimated using Equation (2), and the CM current is measured directly at the reference conductor “G” (see Fig. 14).

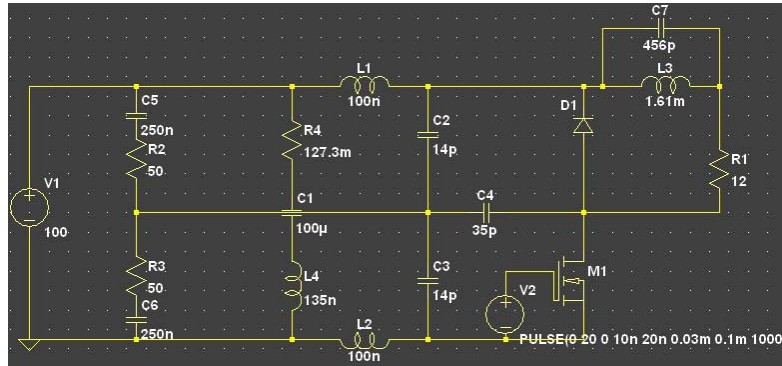


Figure 14. The validation of the buck converter model with LtSpice simulation.

The comparison between spectrums, the model and the Spice simulation are plotted in Fig. 15 (for the DM current) and Fig. 16 (for the CM current). Accordingly, the printed frequencies are the multiple of the switching frequencies (F_{sw}) and the multiple of frequencies equivalent to rising and falling times (t_r and t_f). Since the information amount is stored at the frequencies, one may advance that the agreement is good between the model and Spice simulation results in frequencies point of view. Therefore, we believe that we confirm that the noise’s source developed by the mathematical model is coherent. Regarding the difference of 6 dB between the two spectrums, this can be attributed — among others — to the Spice inner models such as the serial resistance of the *diode* and the *Mosfet*, which are not accounted in the serial impedance expression model “ Z_s ”. Concerning the CM case, we note another resonance around 29 MHz, which we believe that it is due to capacitances to the ground.

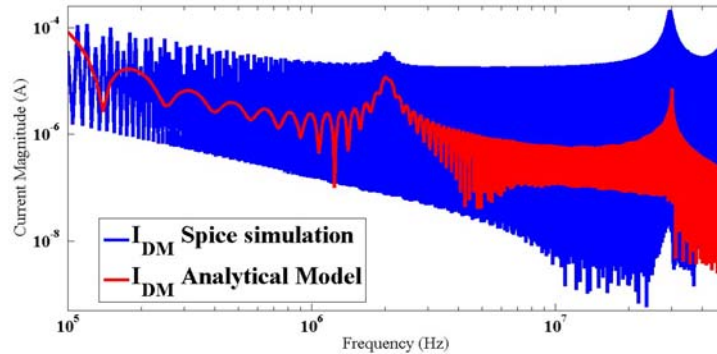


Figure 15. The comparison between the theoretical result (red colour) and the Spice simulation (blue colour) of the differential mode current of the Buck converter.

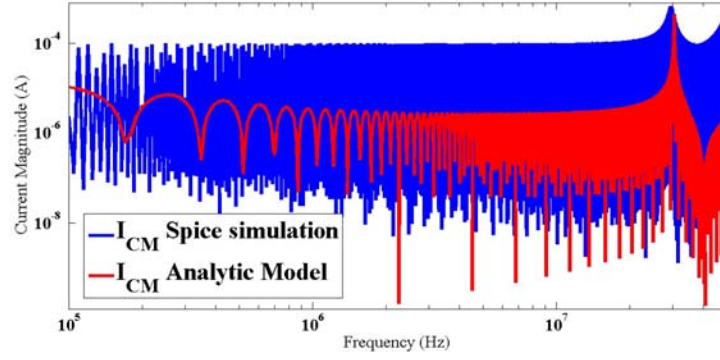


Figure 16. The comparison between the theoretical result (red colour) and the spice simulation (blue colour) of the common mode current of the Buck converter.

8. THE COUPLING MODE MODEL OF THE CONVERTER

In this part, we will consider the converter as a multiport system (three-port). However, the model is built by a combination between equivalent models of the DM (Fig. 6) and the CM (Fig. 11(a)) [19]. Fig. 17(a) shows the three-port equivalent pre-model of the buck converter. The final model (Fig. 17(b)) including current sources, expresses line currents I_p and I_n as voltages function with V_L and V_N voltages. Model's impedances Z_p , Z_s , Z_{pgs} , Z_{ngs} , Z_{pgp} and Z_{ngp} (Fig. 17(a)) are identified as done for the CM modelling in the “Section V”.

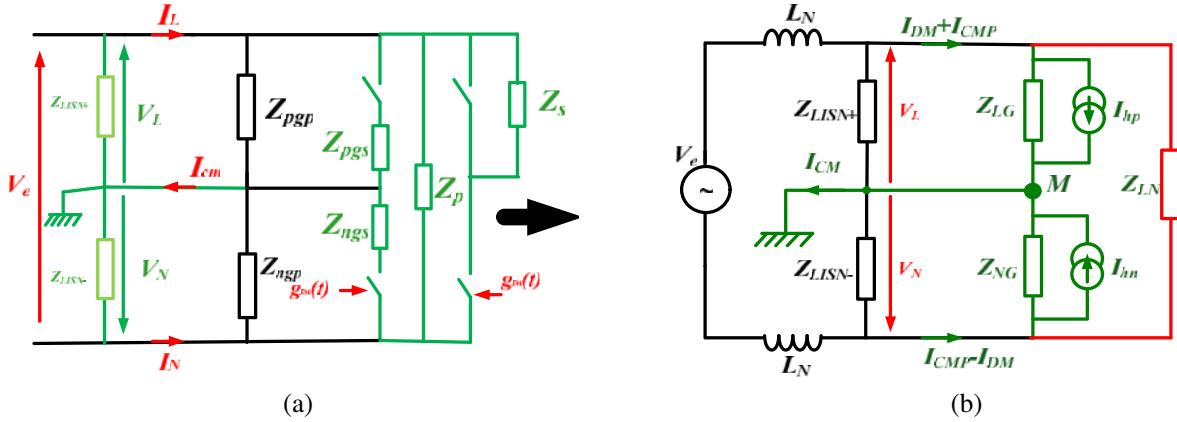


Figure 17. (a) The non decoupling mode model of the converer including switchers. (b) The buck converter quadripolar model after simplifying with the equivalent current sources.

8.1. Analytical Formula

According to Fig. 17(a), lines' currents are expressed as bellow [31]:

$$I_L = I_{CMP} + I_{DM} \quad (30)$$

$$I_N = I_{CMN} - I_{DM} \quad (31)$$

The DM line current I_{DM} and CM line currents (I_{CMP} , I_{CMN}) are built similarly as done for both the DM case and CM case, in Section 3 and Section 5 [28].

$$I_{DM} = Y_{DM} \cdot V_{DM}(f) + I_{DMh}(f) \quad (32)$$

$$I_{cmp} = (Y_{pgp} + Y_{pgs}) \cdot V_L - Y_{pgs} \cdot (G(f) \otimes V_L) = Y_{LG} \cdot V_L(f) + I_{hp} \quad (33)$$

$$I_{cmn} = Y_{ngp} \cdot V_N + Y_{ngs} \cdot (G(f) \otimes V_N) = Y_{NG} \cdot V_N(f) + I_{hn} \quad (34)$$

Harmonic sources are expressed below coming from the convolution product development in Eqs. (32)–(34).

$$I_{DMh} = 2\alpha^2 \cdot \sum_{n \neq 0} \sum Y_s(f - nF_{sw}) \sin c(\pi n\alpha) \cdot \sin c(\pi k\alpha) e^{-j\pi\alpha(n+k)} \cdot V_L(f - (n+k) \cdot F_{sw}) \quad (35)$$

$$I_{hpg} = -\alpha \cdot Y_{pgs} \cdot \sum_{n \neq 0} \sin c(\pi n\alpha) \cdot e^{-j\pi\alpha n} \cdot V_L(f - n \cdot F_{sw}) \quad (36)$$

$$I_{hng} = \alpha \cdot Y_{ngs} \cdot \sum_{n \neq 0} \sin c(\pi n\alpha) \cdot e^{-j\pi\alpha n} \cdot V_N(f - n \cdot F_{sw}) \quad (37)$$

Model impedances described in Fig. 17(b) are expressed bellow, with impedances previously identified in Fig. 10 and Fig. 12.

$$Y_{LN} = Y_p + \alpha^2 \cdot \sum_n \frac{\sin c^2(\pi \cdot \alpha \cdot n)}{Z_s(f - n \cdot F_{sw})} \quad (38)$$

$$Y_{LG} = Y_{pgp} + (1 - \alpha) \cdot Y_{ngs} \quad (39)$$

$$Y_{NG} = Y_{ngp} + \alpha \cdot Y_{ngs} \quad (40)$$

Finally, lines' currents expressions can be formulated as in (41)–(42):

$$I_L = V_L \cdot Y_{LG} + V_{DM} \cdot Y_{DM} + I_{hpg} + 2 \cdot I_{DMh} \quad (41)$$

$$I_N = V_N \cdot Y_{NG} - V_{DM} \cdot Y_{DM} + I_{hng} - 2 \cdot I_{DMh} \quad (42)$$

8.2. Time Domain Simulation

The DC-converter is simulated under *LtSpice* software (Fig. 14). The comparison between both lines' current computed by the model build under the non-decoupling mode assumption (Equation (41)–(42)) and the line current extracted by simulation under *LtSpice* software is shown in Fig. 18. As a result, for the same reason outlined previously, the comparison of the results shows a good agreement in frequencies

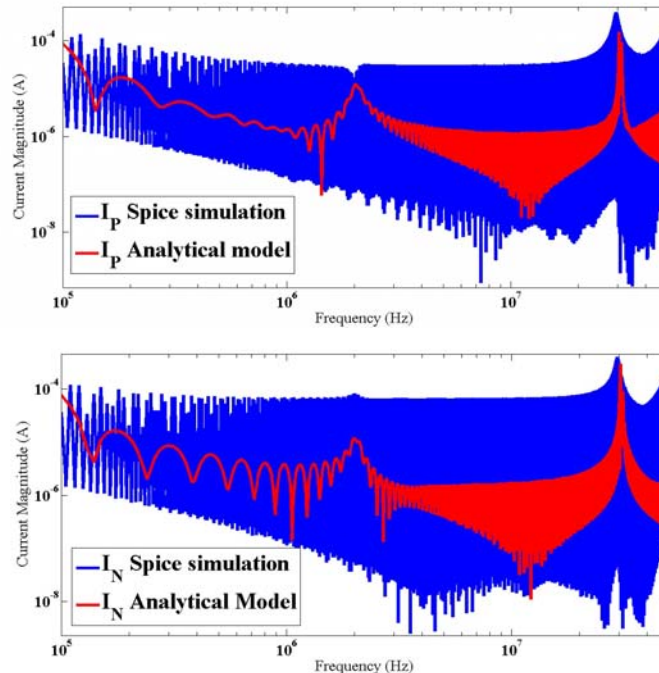


Figure 18. Comparison between line's currents: (blue) analytical result, (red) LtSpice simulation.

point of view. Note that the resonance of 29 MHz recorded previously (Figs. 15–16) appears also in this case, due to the impedance increase in this frequency (Figs. 12–13).

9. THE MATHEMATICAL MODEL AT THE NETWORK LEVEL

As mentioned previously, converters in operation inside an electrical grid inject harmonic currents or voltages (CM and DM components) — as demonstrated in the two models (25) and (3) — which propagate inside the cables, causing new resonances and EMC constraints, and then complicate the EMI filters role. For this reason and to optimise the filter design, in which its *insertion loss* depends on the upstream and downstream impedance of the network, it is important to build models at the network level, accounting for converters, cables, and geometrical physical parameters. The aim in this part is to predict the noise current inside a simple defined network (Fig. 1). The converter emits a noise current, which will be computed at any point connected to the network (Fig. 1).

9.1. Differential Mode Model of the Network

Figure 19 shows a DM synoptic diagram of the network under study. The equations governing a *lossless two-conductor line*, connected to the load (the converter model in this case) taking into account the propagation phenomena are shown below in Eqs. (43)–(45).

$$\begin{pmatrix} V(0) \\ I(0) \end{pmatrix} = \begin{pmatrix} V_{dm} \\ I_{dm} \end{pmatrix} = [\Phi] \cdot \begin{pmatrix} V_e(l) \\ I_e(l) \end{pmatrix} \tag{43}$$

$$[\Phi] = \begin{bmatrix} \cos(\beta \cdot l) & -jZ_c \sin(\beta \cdot l) \\ -j\frac{\sin(\beta \cdot l)}{Z_c} & \cos(\beta \cdot l) \end{bmatrix} \tag{44}$$

$$Z_c = \sqrt{\frac{L_i}{C_i}}, \quad \beta = j\omega\sqrt{L_i \cdot C_i} \tag{45}$$

where:

- $V(0)$ (which is V_{dm}) is the DM voltage at the input sides of the network (Fig. 19);
- $I(0)$ (which is I_{dm}) is the DM current at the input sides of the network (Fig. 19);
- $V_e(l)$ is the voltage at the input sides of the converter (Fig. 19);
- $I_e(l)$ is the current at the input sides of the converter (Fig. 19);
- Φ is the chain matrix [21];
- Z_c is the characteristic impedance;
- β is the propagation parameter;
- L_i is the length per-unit inductance of the cable;

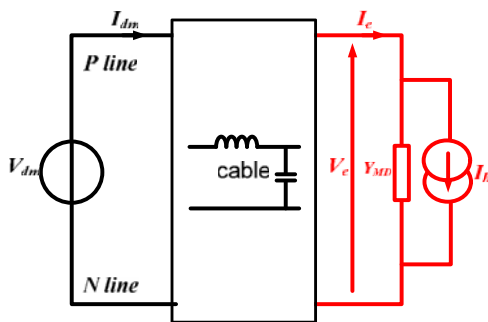


Figure 19. The DM synoptic diagram of the laboratory network under study.

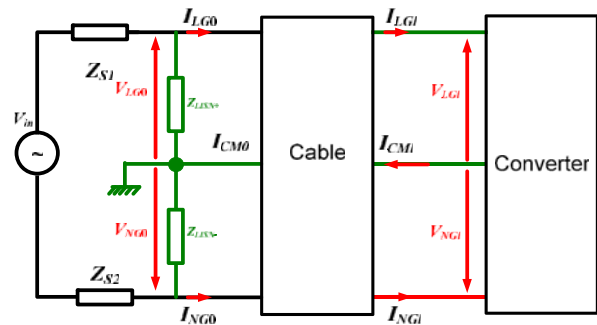


Figure 20. The CM synoptic diagram of the laboratory network under study.

- C_i is the length per-unit capacitance of the cable;
- ω is the signal frequency propagating inside the cable;
- r_i : is the per-unit resistance of the TL;
- l is the cable length between the power source and the converter.

9.2. Common Mode Model of the Network

Figure 20 shows a CM synoptic diagram of the network under study, including the converter model represented by the CM current sources (I_{hp} and I_{hn}). The equations governing transmission lines of a lossless multi-conductor, connected to the load (the converter model in this case) taking into account the propagation phenomena are shown below in Eqs. (46)–(49) [31].

$$\begin{pmatrix} \hat{V}(l) \\ \hat{I}(l) \end{pmatrix} = \begin{pmatrix} V_{LGl} \\ V_{NGl} \\ I_{LGl} \\ I_{NGl} \end{pmatrix} = [\Phi] \cdot \begin{pmatrix} \hat{V}(0) \\ \hat{I}(0) \end{pmatrix} = [\Phi] \cdot \begin{pmatrix} V_{LG0} \\ V_{NG0} \\ I_{LG0} \\ I_{NG0} \end{pmatrix} \quad (46)$$

$$[\Phi] = \begin{bmatrix} [\phi_1] & [\phi_2] \\ [\phi_4] & [\phi_3] \end{bmatrix} \quad (47)$$

$$Z_c = \sqrt{\frac{L_i}{C_i}} \quad (48)$$

$$\beta = j\omega\sqrt{L_i C_i} \quad (49)$$

where:

- V_{LG0} is the voltage at input sides of the network (Fig. 20);
- V_{NG0} is the voltage at input sides of the network (Fig. 20);
- I_{LG0} is the line current at input sides of the network (Fig. 20);
- I_{NG0} is the line current at input sides of the network (Fig. 20);
- V_{LGl} is the voltage at terminal sides of the converter (Fig. 20);
- V_{NGl} is the voltage at terminal sides of the network (Fig. 20);
- I_{LGl} is the line current at terminal sides of the network (Fig. 20);
- I_{NGl} is the line current at terminal sides of the network (Fig. 20);
- $[\Phi]$ is the chain matrix, composed by four sub-matrix $[\Phi_1]$, $[\Phi_2]$, $[\Phi_3]$ and $[\Phi_4]$ [21].
- L_i is the length per-unit inductance of the cable;
- C_i is the length per-unit mutual capacitance of the cable;
- ω is the signal frequency propagating inside the cable;
- l is the cable length.

According to Eq. (25), the CM current at the input sides of the converter (at the distance “ $x = l$ ” far from the source) is expressed bellow:

$$I_{CMl} = Y_{LG}V_{LGl} + Y_{NG}V_{NGl} + I_{hp} - I_{hn} \quad (50)$$

According to Equation (46), one can compute the CM current circulating inside the network’s cable at any defined distance “ x ”. By the way, the CM current at the input side of the network ($x = 0$), according to the multi-conductor transmission lines theory, is given bellow [31], where $[\Phi_1]_{11}$ and $[\Phi_1]_{12}$ are the elements of the matrix $[\Phi_1]$ as defined in Eq. (47).

$$I_{CM0} = \frac{I_{CMl}}{[\phi_1]_{11} + [\phi_1]_{12}} \quad (51)$$

10. THE PARAMETER IDENTIFICATION AT THE NETWORK LEVEL

The network under test is composed of a DC power supply connected to the DC converter through a 1 m cable. The converter parameters have been identified in the previous section. In this part, we will identify cable parameters using a multi-conductor transmission line theory.

10.1. Cable Identification Parameter

The network under study has the architecture of Fig. 1. It is composed by the converter previously modelled (Fig. 3), connected to the DC power supply by a 1 m cable (Fig. 21). As mentioned in “Section 3 and 4”, each model (The DM and CM) is studied separately. In other words, when we study the DM case, there is no CM component, and this is also true for the CM case. Consequently, the two conductors’ cable is used for the DM case; however, the three conductors’ cable is used for the CM modeling. The cable is characterised by the impedance analyser “WK 6500B”, using two experimental cases (A and B) as done in [17]. This characterisation leads to providing primary parameters of the cable and is introduced to both; the DM/CM model and time domain simulation are illustrated in Fig. 22 and Fig. 23.

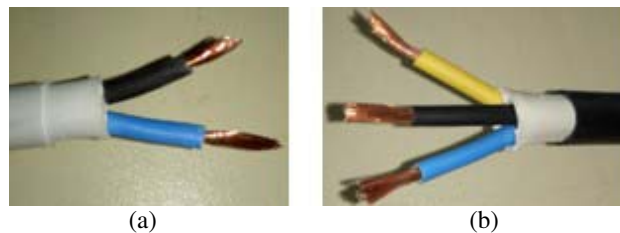


Figure 21. Power cable used for the parameter identification: (a) two-conductor cable for the DM model, (b) three-conductor cable for the CM model.

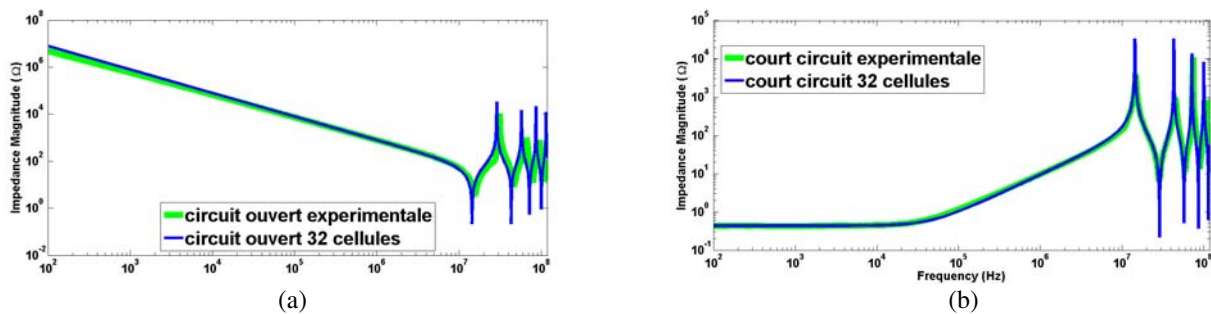


Figure 22. Parameters’ identification with an experimental measurement for the two-conductor cable: (a) open circuit, (b) short-circuit.

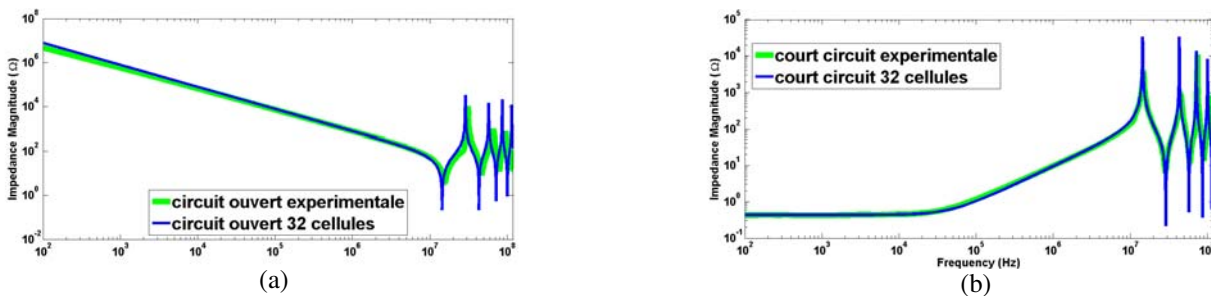


Figure 23. Parameters’ identification with an experimental measurement for the three-conductor cable: (a) open circuit, (b) short-circuit.

11. TIME DOMAIN SIMULATION

In order to test the network model built in Eqs. (43) and (46), we have realised an *LtSpice* simulation about the network as presented in Fig. 24.

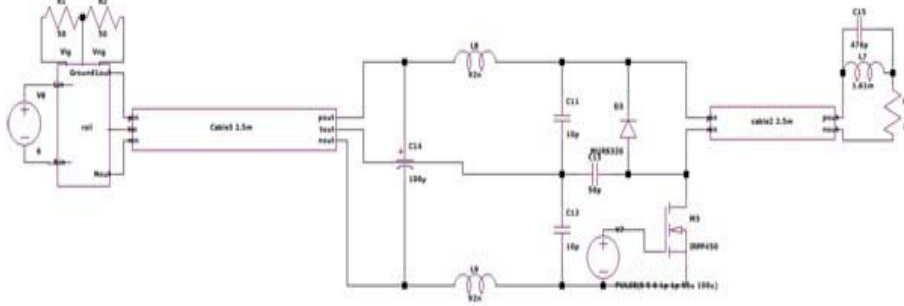


Figure 24. The network scheme of the time domain simulation.

11.1. DM Network Simulation

The simulation for the DM case is done under the following operation points: Input DC voltage: $E = 60\text{ V}$, switching frequency: $F_{Sw} = 10\text{ kHz}$, duty cycle: $\alpha = 0.3$. It is worth noting that since there is a lot of model's data (a lot of points when sampling the analytical model), we have only chosen useful components (just maxima) and then been interpolated by a linear interpolation. This may be clarified with the following analytical development. Hence, since the input voltage $v_e(t)$ is a DC supply, its expression can be developed as in Eq. (52):

$$v_e(t) = \frac{E}{2} \cdot (1 + \text{sgn}(t)) \quad (52)$$

where $\text{sgn}(t)$ is the *sign function*, because $v_e(t)$ is causal. Fourier transform of Eq. (52) gives two components, as describe in Eq. (53):

$$V_e(f) = \frac{E}{2} \cdot \delta(f - (n + k) \cdot F_{sw}) + \frac{E}{2} \cdot \frac{1}{j \cdot \pi \cdot (f - (n + k) \cdot F_{sw})} \quad \text{when } f \neq (n + k)F_{sw} \quad (53)$$

According to Eq. (53), the second term has no information for the voltage spectrum, and only the first one shows the maxima which are the useful information for any spectrum profile. Therefore, in order to reduce sampling points' numbers, we are not forced to take the second term of Eq. (53).

The discussing results, between the model $I_{dm}(f)$ expressed in Eq. (43) and *LtSpice* simulation are plotted in Fig. 25. One notes that the frequencies of the model and Spice results are matched especially for the two resonance frequencies around 2 MHz and 29 MHz. This confirms that the noise's source developed by the mathematical model within the network is sufficiently coherent.

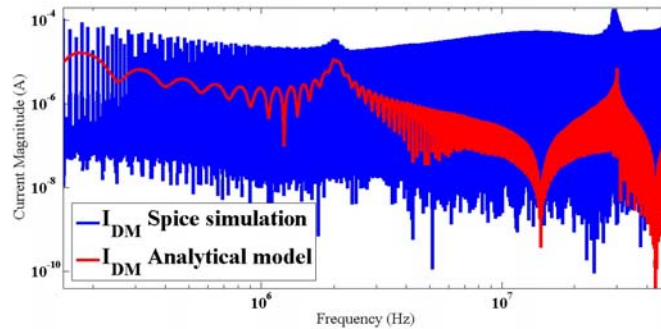


Figure 25. The comparison between the analytical result (Red colour) and the spice simulation (blue colour) of the DM current inside the network.

11.2. CM Network Simulation

The whole system, composed by the DC-source connected to the previous converter through a 1 m cable, is simulated by *LtSpice* software, in order to compute the CM current at the input sides of the network (I_{CM0}). Let's not forget the initial purpose of this work which is the noise current prediction inside the network at any point. As presented in Fig. 21, the cable is modelled by the MTL model given by *LtSpice* software. The cell number, introduced at the *LtSpice* software, makes a decision on the model accuracy [20], but it is limited by the simulation convergence.

Figure 26 shows the comparison between the analytical model spectrum and the *Spice* simulation of the CM current at the input side of the network. Note that there is almost a good consistency between the analytical model (blue colour) and the time domain simulation (red colour). Another point that should be made in evidence is that the CM current computed in this case including the cable is totally different from that computed for the converter case alone without the cable (Fig. 16).

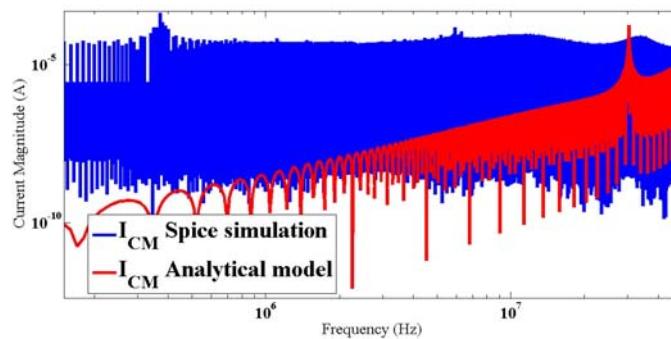


Figure 26. CM current at input sides of the network: (blue colour) Time domain simulation, (red colour) the model developed by the MTL theory.

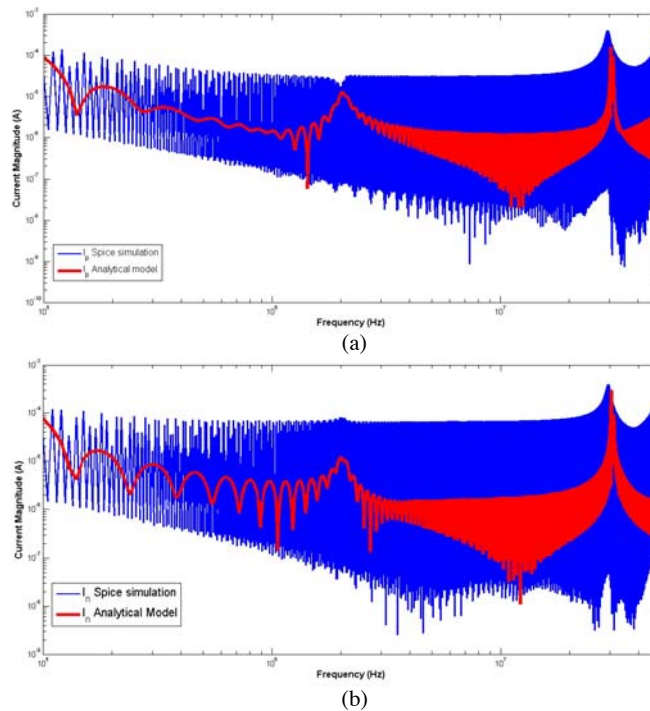


Figure 27. The current at the input sides of the network: (a) The current at the line “P”. (b) The current at the line “N”.

Lines' currents I_{LG0} and I_{NG0} (Fig. 20) have been computed by the model (Equation (46)). Fig. 27 shows the comparison between analytical model and *Spice* simulation of both P -line and N -line currents at the input sides of the network (Fig. 20). The results show a good agreement in frequency point of view and prove that the model developed, thanks to the TLM, is efficient to predict conducted noise current generated by converters connected to the grid.

12. CONCLUSIONS

In this paper, we have worked out an experimental and simulation study on a simple network including a DC-DC converter, on both the DM and CM references. Firstly, we have modelled the converter by an equivalent Norton circuit, including noise sources current and switching impedances. The model parameters are identified by mean experimental measurements. The constructed model, based on experimental parameters identification is validated by a time domain simulation using *LTSpice*. Secondly, a Buck converter has been inserted in an elementary network in order to quantify how the noise current behaves inside this network. Thus, the whole network, composed by the source, the cable and the converter is modelled by a multi-conductor transmission line theory. The network model is identified by experimental measurements. As a consequence, we have compared this model with a time domain simulation, and it is validated by experimental measurements from a few Hz to tens of MHz. Finally, it is worth pointing out that the noise current circulating inside network's cables creates new resonances due to the cables' parameters, which make the EMI filter role more and more difficult.

REFERENCES

1. Marlier, C. A. Videt, and N. Idir, "NIF-based frequency-domain modeling of three-wire shielded energy cables for EMC simulation," *IEEE Transaction on Electromagnetic Compatibility*, Vol. 57, 145–155, 2015.
2. Musznicki, P., "Conducted EMI propagation paths in DC-AC hard switching converter," *International Review of Electrical Engineering*, Vol. 8, 1870–1875, 2013.
3. Ales, A., M. A. Cheurfi Belhadj, J.-L. Schanen, and A. Zaoui, "Analytical models of EMI sources for power electronic converters," *International Conference on Environment and Electrical Engineering*, 2017.
4. Guo, Y. J., L. Wang, and C. Liao, "Systematic analysis of conducted electro-magnetic interferences for the electric drive system in electric vehicles," *Progress In Electromagnetics Research*, Vol. 134, 359–378, 2013.
5. Guo, Y. J., L. F. Wang, and C. L. Liao, "Modeling and analysis of conducted electromagnetic interference in electric vehicle power supply system," *Progress In Electromagnetics Research*, Vol. 139, 193–209, 2013.
6. Kirchhof, Y. and J. Zhang, "A new EMC DC line impedance stabilization network," *26th European Photovoltaic Solar Energy Conference and Exhibition*, 3735–3738, 2011.
7. Gu, B., J. Dominic, J.-S. Lai, C.-L. Chen, T. LaBella, and B. Chen, "High reliability and efficiency single-phase transformerless inverter for grid-connected photovoltaic systems," *IEEE Trans. Power Electron.*, Vol. 28, 2235–2245, 2013.
8. Zaidi, B., A. Videt, and N. Idir, "Design method for the minimization of CM inductor volume with consideration of core saturation in EMI filters," *PCIM Europe*, 464–471, 2017.
9. Hou, C.-C., C.-C. Shih, P.-T. Cheng, and A. M. Hava, "Common-mode voltage reduction pulse width modulation techniques for three-phase grid-connected converters," *IEEE Transaction on Power Electronics*, Vol. 28, 1971–1979, 2013.
10. Rucinski, M., P. J. Chrzan, P. Musznicki, J.-L. Schanen, and A. Labonne, "Analysis of electromagnetic disturbances in dc network of grid connected building-integrated photovoltaic system," *9th International Conference on Compatibility and Power Electronics*, 332–336, 2015.

11. Zaidi, B., A. Videt, and N. Idir, "Design method for the minimization of common-mode inductor volume taking into account saturation issues in EMI filters for variable duty cycle applications," *19th European Conference on Power Electronics and Applications*, 2017.
12. Saber, C., D. Labrousse, B. Revol, and A. Gascher, "A combined CM & DM conducted EMI modeling approach," *EMC EUROPE*, 2017.
13. Hefner, A. R. and D. M. Diebolt, "An experimentally verified IGBT model implemented in the Saber circuit simulator," *IEEE Transactions on Power Electronics*, Vol. 9, 532–542, 1994.
14. Foissac, M., J. L. Schanen, and C. Vollaie, "Black box EMC model for power electronics," *IEEE Energy Conversion Congress and Exposition*, 3609–3615, 2009.
15. Labrousse, D., B. Revol, F. Costa, "Common mode modeling of the association of n-switching cells: Application to an electric-vehicle-drive system," *IEEE Transactions on Power Electronics*, Vol. 25, 2852–2859, 2010.
16. Liu, Q., F. Wang, and D. Boroyevich, "Modular-terminal-behavioral model for characterizing switching module conducted EMI generation in converter systems," *IEEE Transactions on Power Electronics*, Vol. 21, 1804–1814, 2006.
17. Ales, A., J. L. Schanen, D. Moussaoui, and J. Roudet, "Impedances identification of DC/DC converters for network EMC analysis," *IEEE Transactions on Power Electronics*, Vol. 29, 6445–6457, 2014
18. Jettanasen, C., F. Costa, and C. Vollaie, "Common-mode emissions measurements and simulation in variable-speed drive systems," *IEEE Transactions on Power Electronics*, Vol. 24, 2456–2464, 2009.
19. Ales, A., J. L. Schanen, D. Moussaoui, and J. Roudet, "A new analytical EMC model of power electronics converters based on quadripole system: Application to demonstrate the mode decoupling condition," *The Applied on Power Electronics Conference and Exposition*, 2015.
20. Bishnoi, H., P. Mattavelli, R. Burgos, and D. Boroyevich, "EMI behavioral models of DC-fed three-phase motor drive systems," *IEEE Transaction on Power Electronics*, Vol. 29, 4633–5645, 2014.
21. Paul, C. R., *Analysis of Multiconductor Transmission Lines*, Wiley-Interscience, USA, 1994.
22. Kherif, O., S. Chiheb, M. Tegar, A. Mekhaldi, and N. Harid, "Time-domain modeling of grounding systems' impulse response incorporating nonlinear and frequency-dependent aspects," *IEEE Transactions on Electromagnetic Comaptibility*, Vol. 60, 907–916, 2017.
23. Xie, H., J. Wang, R. Fan, and Y. Liu, "Spice models to analyze radiated and conducted susceptibilities of shielded coaxial cables," *IEEE Transactions on Electromagnetic Comaptibility*, Vol. 52, 215–222, 2010.
24. Zaidi, B., A. Videt, and N. Idir, "Influence of switching frequency and saturation of the magnetic material on the volume of common-mode inductors used in power converter EMI filters," *IEEE Energy Conversion Congress and Exposition*, 2017.
25. Laour, M., R. Tahmi, C. Volaie, "Modeling and analysis of conducted and radiated emission due to common mode current of a buck converter," *IEEE Transactions on Electromagnetic Compatibility*, Vol. 59, 1260–1267, 2017.
26. Yang, L., G. N. Wu, and X. B. Cao, "An optimized transmission line model of grounding electrodes under lightning currents," *Sci. China Tech. Sci.*, Vol. 56, 335–341, 2013,
27. Bishnoi, H., A. C. Baisden, P. Mattavelli, and D. Boroyevich, "Analysis of EMI terminal modeling of switched power converters," *IEEE Transactions on Power Electronics*, Vol. 27, 3924–3933, September 2012.
28. Ales, A., M. A Cheurfi Belhadj, A. Zaoui, and J. L. Schanen, "Analytical model of emi sources on the network level including power electronics converters," *EPE'2017 ECCE Europe*, Warsaw, Poland, Septembre 2017.
29. Frantz, G., D. Frey, J.-L. Schanen, H. Bishnoi, and P. Mattavelli, "EMC models for power electronics: From converter design to system level," *Energy Conversion Congress and Exposition (ECCE)*, 2013 IEEE, Denver CO, September 15–19, 2013.

30. Poon, N. K., B. M. H. Pong, C. P. Liu, and C. K. Tse, "Essential-coupling-path models for non contact EMI in switching power converters using lumped circuit elements," *IEEE Transactions on Power Electronics*, Vol. 18, 686–695, March 26, 2003.
31. Cheurfi Belhadj, M. A., A. Ales, A. Zaoui, Z. Chebbat, J. L. Schanen, and J. Roudet, "Analytical model of DC-DC converters based on switching impedances and EMI sources," *EMC Europe 2016, Wroclaw 2016*, Poland, September 2016.